

Evolution of the Fermi surface in superconductor $\text{PrO}_{1-x}\text{F}_x\text{BiS}_2$ ($x=0.0, 0.3$, and 0.5) revealed by angle-resolved photoemission spectroscopy

T. Morita,¹ Y. Matsuzawa,¹ S. Kumar²,³ E. F. Schwier,² K. Shimada,² R. Higashinaka,³ T. D. Matsuda,³ Y. Aoki³,³ N. L. Saini,⁴ and T. Mizokawa¹

¹Department of Applied Physics, Waseda University, Tokyo 169-8555, Japan

²Hiroshima Synchrotron Radiation Center, Hiroshima University, Higashihiroshima 739-0046, Japan

³Department of Physics, Tokyo Metropolitan University, Hachioji 192-0397, Japan

⁴Dipartimento di Fisica, Università di Roma "La Sapienza," Piazzale Aldo Moro 2, 00185 Rome, Italy



(Received 16 September 2020; revised 27 January 2021; accepted 23 February 2021; published 16 March 2021)

We have investigated the electronic structure evolution with F doping in $\text{PrO}_{1-x}\text{F}_x\text{BiS}_2$ ($x = 0.0, 0.3, 0.5$) by means of angle-resolved photoemission spectroscopy. Undoped PrOBiS_2 exhibits Fermi surface (FS) pockets around the X point which can be associated with electron doping due to the $\text{Pr}^{3+}/\text{Pr}^{4+}$ mixed valence. At $x = 0.3$, the FS pockets are expanded, and their area is almost consistent with the F doping level. Interestingly, horizontal segments facing each other in the rectangular FS pockets lose their spectral weight. The partial suppression of the FS pockets suggests possible anisotropic charge fluctuations around $x = 0.3$. At $x = 0.5$, the FS area is much smaller than the expected value as commonly observed for $\text{CeO}_{0.5}\text{F}_{0.5}\text{BiS}_2$ and $\text{NdO}_{0.5}\text{F}_{0.5}\text{BiS}_2$. In addition, the highly depleted spectral weight at the FS pockets would be consistent with evident charge fluctuations driven by atomic disorder in the BiS_2 network.

DOI: [10.1103/PhysRevB.103.094510](https://doi.org/10.1103/PhysRevB.103.094510)

I. INTRODUCTION

The discovery of a BiS_2 -based superconductor by Mizuguchi *et al.* [1] has been followed by extensive experimental and theoretical studies on BiS_2 -based superconductors [2]. The $\text{Bi } 6p_x/6p_y$ orbitals form a multiband Fermi surface (FS) in the BiS_2 layer and provide an interesting platform for the study of the superconductivity [3,4]. Among the various BiS_2 -based superconductors, $\text{RO}_{1-x}\text{F}_x\text{BiS}_2$ (R =rare earth element) systems have been investigated by means of various experimental and theoretical techniques [5–20]. In a typical $R(\text{O,F})\text{BiS}_2$ system, the F substitution for O in the $R(\text{O,F})$ layer introduces electrons to the electronically active BiS_2 layer (Fig. 1). The superconducting transition temperature T_c at ambient pressure increases in going from $R = \text{La}$ to $R = \text{Nd}$ [2]. The FSs and the band dispersions of $R(\text{O,F})\text{BiS}_2$ have been investigated by means of angle-resolved photoemission spectroscopy (ARPES) [22–27]. Since electronic correlation is expected to be weak in the $\text{Bi } 6p$ bands, the observed band structure and FS geometry were considered to be basically consistent with the band structure calculations. However, there is a serious discrepancy between the doping level and the observed FS area for $\text{CeO}_{0.5}\text{F}_{0.5}\text{BiS}_2$ [26] and $\text{NdO}_{0.5}\text{F}_{0.5}\text{BiS}_2$ [22], while they seem consistent in $\text{LaO}_{0.5}\text{F}_{0.5}\text{BiS}_2$ [24]. In addition, a laser ARPES study on $\text{NdO}_{0.71}\text{F}_{0.29}\text{BiS}_2$ has revealed a highly anisotropic superconducting gap, indicating the pairing mechanism is unconventional [28].

The Bi site is pyramidally coordinated by four in-plane sulfur atoms (S1) and one apical sulfur atom (S2). The electronic structure of the BiS_2 layer is strongly affected by the coexistence of different local structural configurations with

two distinct Bi-S1 distances [29–31]. The difference in the Bi-S1 distances in the BiS_2 layer is significant with larger R ions such as La [31–33], Ce [34], and Pr [35], while it is reduced with smaller R ions [36] or with Se substitution for S [37]. On the other hand, the interaction between the BiS_2 layer and the R ion is governed by the Bi-S2 distance. The Bi-S2 distance tends to decrease with reducing the R ion radius [36], indicating that the interaction between the BiS_2 layer and the R ion is larger for $R = \text{Pr}$ than $R = \text{Ce}$. Nevertheless, it still remains unclear how the atomic disorder with the coexistence of different local structural configurations is related to the superconducting properties.

Among the $\text{RO}_{1-x}\text{F}_x\text{BiS}_2$ systems, the electronic structure of $\text{PrO}_{1-x}\text{F}_x\text{BiS}_2$ [38–41] is not well explored. In contrast to $\text{LaO}_{1-x}\text{F}_x\text{BiS}_2$ with tetragonal and monoclinic phases, $\text{PrO}_{1-x}\text{F}_x\text{BiS}_2$ keeps the tetragonal structure under ambient pressure just like Ce and Nd systems [2,42]. As for the comparison between Ce and Pr systems, both CeOBiS_2 and PrOBiS_2 exhibit a mixed valence of $\text{Ce}^{3+}/\text{Ce}^{4+}$ and $\text{Pr}^{3+}/\text{Pr}^{4+}$, respectively. However, it has been confirmed that the ratio of Pr^{4+} to Pr^{3+} is not sensitive to F doping [40,41], while the ratio of Ce^{4+} to Ce^{3+} decreases with F doping [16]. Therefore, the case of $\text{PrO}_{1-x}\text{F}_x\text{BiS}_2$ is interesting for studying electronic structure evolution by F doping without the valence change in R ions. In this work, we have performed ARPES measurements for $\text{PrO}_{1-x}\text{F}_x\text{BiS}_2$ ($x = 0.0, 0.3$, and 0.5). Since the mixed-valence behaviors of the Ce and Pr systems are different under F doping, it is expected that the F doping will differentiate the electronic structures of these two systems. However, even at $x = 0.0$, PrOBiS_2 exhibits FS pockets around the X points, while CeOBiS_2 does not. In

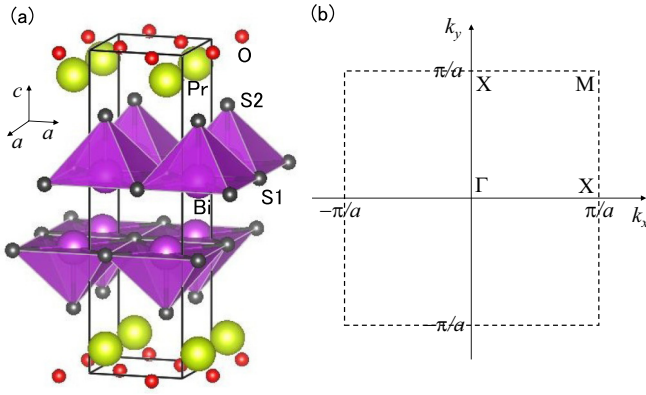


FIG. 1. (a) Crystal structure of PrOBiS₂ created by VESTA [21]. (b) Two-dimensional Brillouin zone of PrO_{1-x}F_xBiS₂.

going from $x = 0.0$ to 0.3 , the FS pockets of PrO_{1-x}F_xBiS₂ are expanded, and their horizontal segments lose their spectral weight. These results suggest that the FS features are affected by possible charge fluctuations, likely driven by peculiar local atomic disorder in these materials.

II. METHOD

High-quality single crystals of PrO_{1-x}F_xBiS₂ ($x = 0.0$, 0.3 , and 0.5) were prepared by the CsCl flux method [20]. The ARPES measurements with linearly polarized photons were performed at the undulator beamline BL-1 [43] of the Hiroshima Synchrotron Radiation Center, Hiroshima University, equipped with a VG SCIENTA R4000 analyzer [44]. The photon energy was set to be 30 eV for all the polarizations. The single-crystalline samples were cleaved *in situ* at 30 K in ultrahigh vacuum ($< 1 \times 10^{-10}$ Torr) in order to obtain a clean (001) surface. The total energy resolution including both the monochromator and electron energy analyzer was measured to be ~ 20 meV. All the measurements were taken at 30 K.

Generalized gradient approximation (GGA)-based band structure calculations were performed using QUANTUM ESPRESSO 5.30 [45,46]. We employed pseudopotentials of PR.REL-PBE-SPDN-KJPAW_PSL.1.0.0.UPF, O.REL-PBE-N-KJPAW_PSL.1.0.0.UPF, BI.REL-PBE-DN-KJPAW_PSL.1.0.0.UPF, and S.REL-PBE-NL-KJPAW_PSL.1.0.0.UPF for calculations with spin-orbit interaction. Cutoff energy was set to 30 Ry.

III. RESULTS AND DISCUSSION

Figure 2 shows a FS map and a selected band map around the X point of PrOBiS₂. k_x and k_y represent wave numbers along the Bi-Bi directions of the square lattice in the BiS₂ layer (see Fig. 1). The ARPES spectral weight is integrated in the ± 25 meV window relative to the Fermi level. Even without F doping, the Bi 6*p* bands accommodate additional electrons due to the Pr³⁺/Pr⁴⁺ mixed valence [41]. The Bi 6*p* bands are substantially broadened due to possible atomic disorder [31] or strong electron-phonon interaction [23]. Although it is difficult to estimate the FS area quantitatively, its upper limit has been estimated to be 0.03 of the Brillouin zone. Assuming that the two branches of the bilayer split

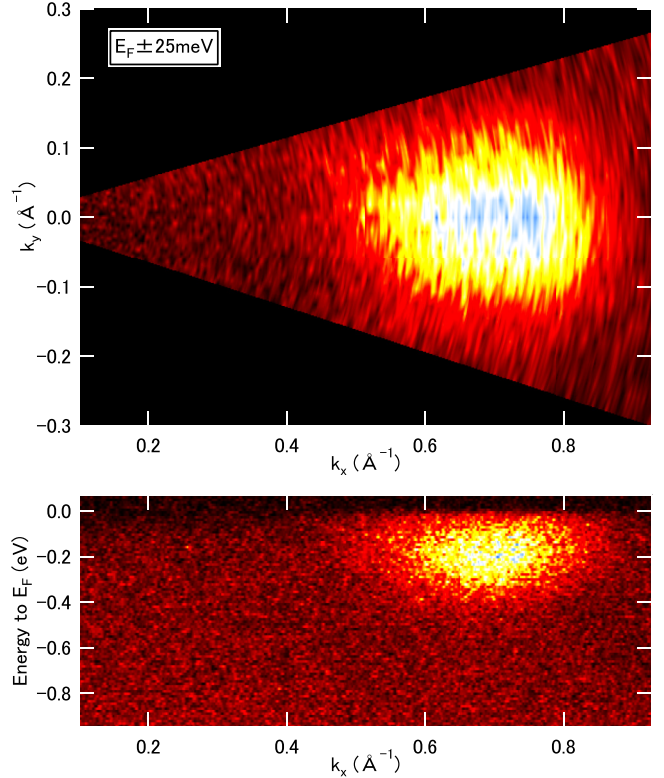


FIG. 2. Top: Fermi surface map for PrO_{1-x}F_xBiS₂ ($x = 0.0$). Bottom: Band map along the Γ -X cut.

Bi 6*p* bands accommodate the electrons, the upper limit of the electron density per Bi is estimated to be 0.06. Here, the bottom of the electron band is located at ~ -0.2 eV in Fig. 2(b).

The present result indicates that PrOBiS₂ can accommodate a homogeneous metallic state due to Bi 6*p* electrons provided by the Pr³⁺/Pr⁴⁺ mixed valence. On the other hand, CeOBiS₂ exhibits inhomogeneous distribution of the minority metallic phase in the majority insulating phase [47]. The difference between CeOBiS₂ and PrOBiS₂ is associated with the interaction between the RO and BiS₂ layers. The lattice constant c is ~ 13.6 \AA for $R = \text{Ce}$ and ~ 13.8 \AA for $R = \text{Pr}$ [20,39], indicating that the separation between the BiS₂ layer and the RO layer increases in going from $R = \text{Ce}$ to $R = \text{Pr}$. In the Ce³⁺/Ce⁴⁺ mixed-valence state for $R = \text{Ce}$, the Ce 4*f* orbitals are hybridized with the Bi 6*p* orbitals via the S 3*p* orbitals at the S2 site. Since this hybridization channel is sensitive to the local displacement of S2, the system tends to be inhomogeneous. On the other hand, in the Pr³⁺/Pr⁴⁺ mixed-valence state for $R = \text{Pr}$, the Pr⁴⁺ state is likely to be due to the hybridization with the O 2*p* orbitals and may not directly affect the Bi 6*p* orbitals. Thus, the Pr⁴⁺ state just seems to provide electrons to the BiS₂ layer.

Figure 3 shows a FS map and selected band maps for $x = 0.3$. Rectangular FS pockets are expected to exist around the X point. The horizontal segments of the FS pockets, however, lose their spectral weight compared to those for the vertical segments. Assuming a rectangular shape, the FS area is estimated to be 0.15 of the Brillouin zone. Since the two branches

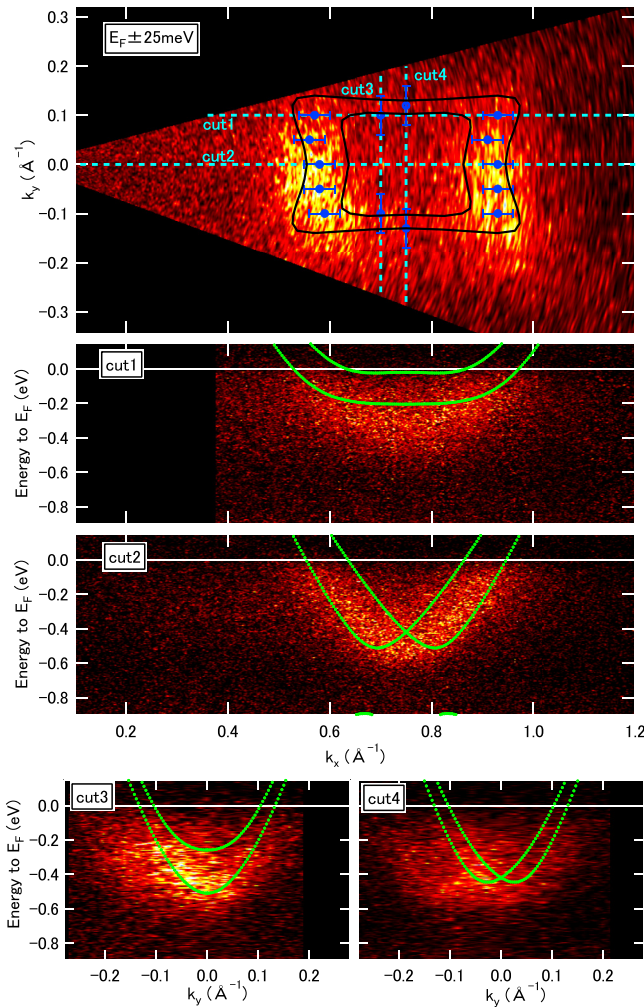


FIG. 3. Top: Fermi surface map for $\text{PrO}_{1-x}\text{F}_x\text{BiS}_2$ ($x = 0.3$). The solid circles indicate the Fermi surface points deduced from momentum distribution curves along the horizontal cuts. The open circles indicate the valence band top points deduced from momentum distribution curves along the vertical cuts. The solid curves indicate calculated Fermi surfaces for 0.3 electron per Bi. Bottom: Band maps along cuts 1, 2, 3, and 4 in the Fermi surface map. The dotted curves indicate calculated band dispersions for 0.3 electron per Bi.

of the bilayer split Bi $6p$ bands accommodate the electrons, the electron density per Bi would be 0.3. Therefore, in going from $x = 0.0$ to 0.3, the electron density per Bi increases from 0.06 to 0.3. This number is almost consistent with the F doping level. In Fig. 3, Fermi surfaces calculated by GGA are indicated by solid curves. The average crystal structure of PrOBiS_2 is employed for the calculation. The Fermi level is set at ~ 0.50 eV from the bottom of the Bi $6p$ band and the number of Bi $6p$ electrons is about 0.3 per Bi. The two Fermi surfaces are derived from the bilayer of BiS_2 . The observed Fermi surface is very broad, and its spectral weight is mainly distributed in the region between the two theoretical Fermi surfaces. The broad spectral distribution in the experimental result is associated with the fact that the local structure is very different from the average crystal structure in $\text{PrO}_{1-x}\text{F}_x\text{BiS}_2$.

The anisotropic spectral weight suppression of the FS pockets in Fig. 3 can be explained if the horizontal segments have orbital components different from those of the vertical segments. Considering the linear polarization (horizontal direction), the horizontal and vertical segments should be the $6p_y$ and $6p_x$ orbitals, respectively. This orbital polarization can be obtained if the vertical segments are constructed from the Bi $6p_x$ band dispersing along the horizontal direction (k_x direction), and the horizontal ones are from the Bi $6p_y$ band. However, such an orbital state with different Bi $6p$ orbital components between the horizontal and vertical segments is not expected from the band structure calculation, which predicts the same orbital component for the horizontal and vertical segments [6]. The theoretical prediction was confirmed by the polarization-dependent ARPES on $\text{CeO}_{1-x}\text{F}_x\text{BiS}_2$ [26]. Although the mixed-valence states of Ce and Pr are different, one can assume that the Bi $6p$ orbital state of the Fermi surfaces is essentially the same between the Ce and Pr systems. Under this assumption, it is unlikely that the spectral suppression of the horizontal segment in $\text{PrO}_{1-x}\text{F}_x\text{BiS}_2$ is derived from differentiation of the Bi $6p$ orbital component between the vertical and horizontal segments.

The other explanation of the anisotropic spectral weight suppression is associated with anisotropic charge fluctuations. Under the influence of such fluctuations, the horizontal segments would be selectively affected and lose their spectral weight due to pseudogap formation. According to theoretical considerations for $x = 0.5$ [6,10], charge fluctuations along the (q, q) direction (the diagonal direction) are expected since FS segments in the diagonal direction or the Γ - M direction are formed due to the heavy electron doping (0.5 electron per Bi). When $q \sim \pi/a$, such charge fluctuations correspond to checkerboard-type charge patterns in which the vertical and horizontal directions are equivalent. At $x = 0.3$, stripe-type charge fluctuations can develop along the $(0, q)$ direction (the vertical direction) associated with the rectangular FS shape around the X point. Indeed, the wave vector difference between the two segments is $q \sim 0.25 \text{ \AA}^{-1}$, which is close to $1/6$ of $2\pi/a$ ($\sim 1.5 \text{ \AA}^{-1}$). Stripe-type charge fluctuations with sixfold periodicity is consistent with the experimental result. Such a mechanism can provide a similar effect in cuprates with anisotropic (stripe-type) charge fluctuation. In electron-doped cuprates, rectangular electron pockets are formed around the X point in the antiferromagnetic phase of the electron-doped CuO_2 layer. At low doping level, the FS pocket is closed and rectangular [48,49]. With increasing electron doping level, two segments of the electron pocket facing each other lose their spectral weight [50,51]. Silva Neto *et al.* pointed out that the wave vectors between the missing segments are associated with the charge fluctuation or charge ordering found by resonant x-ray scattering [52]. Considering the similarity of the missing segments of the rectangular Fermi surfaces, we speculate that the stripe-type charge fluctuation plays a role in BiS_2 systems.

Figure 4 shows a FS map and selected band maps for $x = 0.5$. Rectangular FS pockets are observed around the X point which are similar to $\text{NdO}_{1-x}\text{F}_x\text{BiS}_2$ [22,23] and $\text{CeO}_{1-x}\text{F}_x\text{BiS}_2$ [26]. The area of the rectangular FS pocket is estimated to be 0.13 of the Brillouin zone. Thus, the electron density per Bi would be 0.26. This value is much smaller

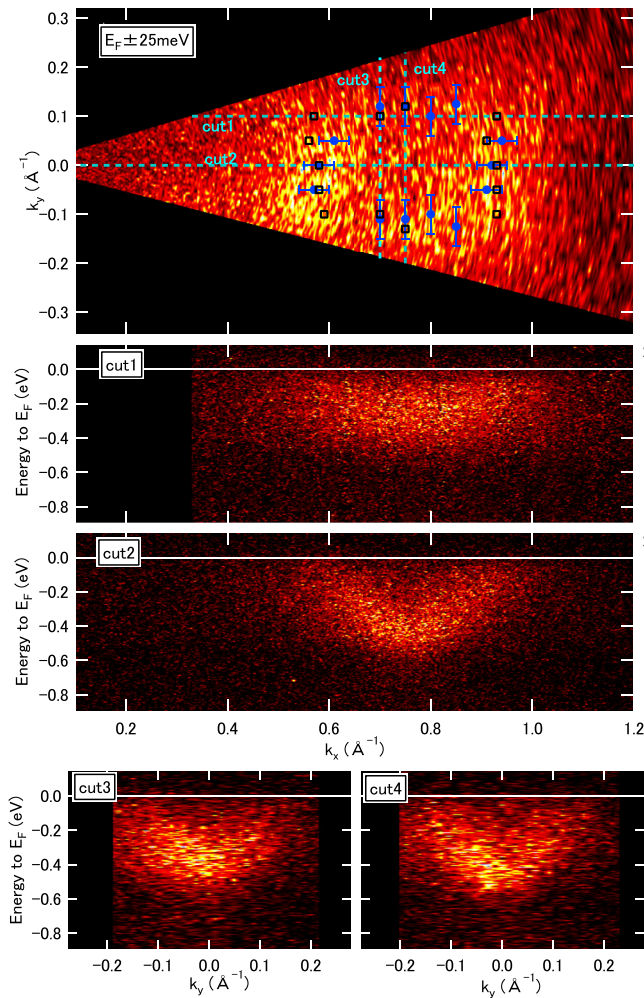


FIG. 4. Top: Fermi surface map for $\text{PrO}_{1-x}\text{F}_x\text{BiS}_2$ ($x = 0.5$). The solid circles indicate the Fermi surface points deduced from momentum distribution curves along the horizontal and vertical cuts. The open squares indicate the Fermi surface points for $x = 0.3$. Bottom: Band maps along cuts 1, 2, 3, and 4 in the Fermi surface map.

than that expected for the F doping of $x = 0.5$. The area reduction and the rectangular shape of the FS pockets are commonly observed in the tetragonal $\text{RO}_{1-x}\text{F}_x\text{BiS}_2$ systems with $x = 0.5$. The bottom of the Bi $6p$ bands is located around -0.5 eV, similar to the value for $x = 0.3$. Although the F content increases from $x = 0.3$ to $x = 0.5$, the FS area and the Bi $6p$ band width do not change appreciably. A possible reason for the reduced FS area is that the doped electrons are reduced by interstitial F and/or by a S vacancy. Another possibility is that the doped electrons are accommodated by Bi $6p_z$ orbitals which are localized and do not contribute to the Fermi surface [47].

In the case of $R = \text{Pr}$, the FS area is saturated for $x > 0.3$, probably because the supplied electrons are grabbed by localized states. With the rectangular Fermi surface for 0.3 electron per Bi, stripe-type charge fluctuations with $Q = (0, \pi/3a)$ are expected. If the BiS_2 layer can accommodate electron concentration up to 0.5 per Bi, the checkerboard-type charge fluctuations with $Q = (\pi/a, \pi/a)$ would become relevant and are expected for $R = \text{La}$ [32]. Indeed, the FS area of $\text{LaO}_{0.5}\text{F}_{0.5}\text{BiS}_2$ is consistent with the F doping level of $x = 0.5$ as reported by Terashima *et al.* [4,24]. In the future, possible interplay between the charge fluctuations and the monoclinic distortion should be clarified experimentally for $\text{LaO}_{0.5}\text{F}_{0.5}\text{BiS}_2$. As for $R = \text{Ce}$, Pr , and Nd , the trapped electrons are expected to induce local atomic disorder in the BiS_2 layer. Such additional atomic disorder may couple with underlying charge fluctuations and may disturb the FS pockets. It would be interesting to study the interplay between charge fluctuations and local atomic disorder in a systematic way for various layered superconductors.

IV. CONCLUSION

We have studied the electronic structure of the $\text{PrO}_{1-x}\text{F}_x\text{BiS}_2$ system for different F doping levels by means of ARPES. The ARPES results on undoped PrOBiS_2 show FS pockets around the X point, which can be associated with the $\text{Pr}^{3+}/\text{Pr}^{4+}$ mixed valence. In $\text{PrO}_{0.7}\text{F}_{0.3}\text{BiS}_2$, the FS area is consistent with the F doping level. Interestingly, two segments facing each other in the rectangular pocket lose their spectral weight at $x = 0.3$. Such behavior is somewhat similar to the antiferromagnetic phase of electron-doped cuprates. The partial suppression of the FS segments suggests possible stripe-type charge fluctuations at $x = 0.3$. In going from $x = 0.3$ to $x = 0.5$, the FS area does not increase, suggesting that $x = 0.3$ is close to the optimal doping. Indeed, in ARPES results for $\text{PrO}_{0.5}\text{F}_{0.5}\text{BiS}_2$, the area of the rectangular FS pockets is much smaller than the value expected for the F doping level as commonly observed for the tetragonal $\text{CeO}_{0.5}\text{F}_{0.5}\text{BiS}_2$ and $\text{NdO}_{0.5}\text{F}_{0.5}\text{BiS}_2$.

ACKNOWLEDGMENTS

The authors acknowledge Prof. Y. Mizuguchi and Prof. Y. Takano for the fruitful discussion and thank T. Asano and T. Nakajima for the sample preparation. The synchrotron radiation experiments were done with the approval of the Hiroshima Synchrotron Radiation Center (Proposal No. 17AG026). We thank the N-BARD, Hiroshima University, for supplying the liquid helium. This work was partially supported by Grants-in-Aid from JSPS (Grants No. 19H01839, No. 19H00659, No. 19K15291) and the CREST program of JST (Grant No. JPMJCR15Q2). N.L.S. was supported by the joint research program of ZAIKEN, Waseda University (Project No. 31010).

[1] Y. Mizuguchi, H. Fujihisa, Y. Gotoh, K. Suzuki, H. Usui, K. Kuroki, S. Demura, Y. Takano, H. Izawa, and O. Miura, *Phys. Rev. B* **86**, 220510(R) (2012).

[2] Y. Mizuguchi, *J. Phys. Soc. Jpn.* **88**, 041001 (2019).

[3] M. Ochi, H. Usui, and K. Kuroki, *J. Phys. Soc. Jpn.* **88**, 041010 (2019).

- [4] K. Terashima, T. Wakita, and T. Yokoya, *J. Phys. Soc. Jpn.* **88**, 041006 (2019).
- [5] S. K. Singh, A. Kumar, B. Gahtori, G. Sharma, S. Patnaik, and V. P. S. Awana, *J. Am. Chem. Soc.* **134**, 16504 (2012).
- [6] H. Usui, K. Suzuki, and K. Kuroki, *Phys. Rev. B* **86**, 220501(R) (2012).
- [7] J. Xing, S. Li, X. Ding, H. Yang, and H.-H. Wen, *Phys. Rev. B* **86**, 214518 (2012).
- [8] D. Yazici, K. Huang, B. D. White, A. H. Chang, A. J. Friedman, and M. B. Maple, *Philos. Mag.* **93**, 673 (2012).
- [9] H. Kotegawa, Y. Tomita, H. Tou, H. Izawa, Y. Mizuguchi, O. Miura, S. Demura, K. Deguchi, and Y. Takano, *J. Phys. Soc. Jpn.* **81**, 103702 (2012).
- [10] T. Yildirim, *Phys. Rev. B* **87**, 020506(R) (2013).
- [11] B. Li, Z. W. Xing, and G. Q. Huang, *Europhys. Lett.* **101**, 47002 (2013).
- [12] K. Deguchi, Y. Mizuguchi, S. Demura, H. Hara, T. Watanabe, S. J. Denholme, M. Fujioka, H. Okazaki, T. Ozaki, H. Takeya, T. Yamaguchi, O. Miura, and Y. Takano, *Europhys. Lett.* **101**, 17004 (2013).
- [13] S. Demura, Y. Mizuguchi, K. Deguchi, H. Okazaki, H. Hara, T. Watanabe, S. J. Denholme, M. Fujioka, T. Ozaki, H. Fujihisa, Y. Gotoh, O. Miura, T. Yamaguchi, H. Takeya, and Y. Takano, *J. Phys. Soc. Jpn.* **82**, 033708 (2013).
- [14] M. Nagao, S. Demura, K. Deguchi, A. Miura, S. Watauchi, T. Takei, Y. Takano, N. Kumada, and I. Tanaka, *J. Phys. Soc. Jpn.* **82**, 113701 (2013).
- [15] C. Morice, E. Artacho, S. E. Dutton, D. Molnar, H.-J. Kim, and S. S. Saxena, *J. Phys.: Condens. Matter* **28**, 345504 (2016).
- [16] T. Sugimoto, B. Joseph, E. Paris, A. Iadecola, T. Mizokawa, S. Demura, Y. Mizuguchi, Y. Takano, and N. L. Saini, *Phys. Rev. B* **89**, 201117(R) (2014).
- [17] M. Nagao, A. Miura, S. Demura, K. Deguchi, S. Watauchi, T. Takei, Y. Takano, N. Kumada, and I. Tanaka, *Solid State Commun.* **178**, 33 (2014).
- [18] T. Machida, Y. Fujisawa, M. Nagao, S. Demura, K. Deguchi, Y. Mizuguchi, Y. Takano, and H. Sakata, *J. Phys. Soc. Jpn.* **83**, 113701 (2014).
- [19] S. Demura, K. Deguchi, Y. Mizuguchi, K. Sato, R. Honjyo, A. Yamashita, T. Yamaki, H. Hara, T. Watanabe, S. J. Denholme, M. Fujioka, H. Okazaki, T. Ozaki, O. Miura, T. Yamaguchi, H. Takeya, and Y. Takano, *J. Phys. Soc. Jpn.* **84**, 024709 (2015).
- [20] R. Higashinaka, T. Asano, T. Nakashima, K. Fushiya, Y. Mizuguchi, O. Miura, T. D. Matsuda, and Y. Aoki, *J. Phys. Soc. Jpn.* **84**, 023702 (2015).
- [21] K. Homma and F. Izumi, *J. Appl. Crystallogr.* **44**, 1272 (2011).
- [22] Z. R. Ye, H. F. Yang, D. W. Shen, J. Jiang, X. H. Niu, D. L. Feng, Y. P. Du, X. G. Wan, J. Z. Liu, X. Y. Zhu, H. H. Wen, and M. H. Jiang, *Phys. Rev. B* **90**, 045116 (2014).
- [23] L. K. Zeng, X. B. Wang, J. Ma, P. Richard, S. M. Nie, H. M. Weng, N. L. Wang, Z. Wang, T. Qian, and H. Ding, *Phys. Rev. B* **90**, 054512 (2014).
- [24] K. Terashima, J. Sonoyama, T. Wakita, M. Sunagawa, K. Ono, H. Kumigashira, T. Muro, M. Nagao, S. Watauchi, I. Tanaka, H. Okazaki, Y. Takano, O. Miura, Y. Mizuguchi, H. Usui, K. Suzuki, K. Kuroki, Y. Muraoka, and T. Yokoya, *Phys. Rev. B* **90**, 220512(R) (2014).
- [25] N. L. Saini, D. Ootsuki, E. Paris, B. Joseph, A. Barinov, M. Tanaka, Y. Takano, and T. Mizokawa, *Phys. Rev. B* **90**, 214517 (2014).
- [26] T. Sugimoto, D. Ootsuki, C. Morice, E. Artacho, S. S. Saxena, E. F. Schwier, M. Zheng, Y. Kojima, H. Iwasawa, K. Shimada, M. Arita, H. Namatame, M. Taniguchi, M. Takahashi, N. L. Saini, T. Asano, R. Higashinaka, T. D. Matsuda, Y. Aoki, and T. Mizokawa, *Phys. Rev. B* **92**, 041113(R) (2015).
- [27] E. Paris, T. Sugimoto, T. Wakita, A. Barinov, K. Terashima, V. Kandyba, O. Proux, J. Kajitani, R. Higashinaka, T. D. Matsuda, Y. Aoki, T. Yokoya, T. Mizokawa, and N. L. Saini, *Phys. Rev. B* **95**, 035152 (2017).
- [28] Y. Ota, K. Okazaki, H. Q. Yamamoto, T. Yamamoto, S. Watanabe, C. Chen, M. Nagao, S. Watauchi, I. Tanaka, Y. Takano, and S. Shin, *Phys. Rev. Lett.* **118**, 167002 (2017).
- [29] Q. Liu, X. Zhang, and A. Zunger, *Phys. Rev. B* **93**, 174119 (2016).
- [30] X. Zhou, Q. Liu, J. A. Waugh, H. Li, T. Nummy, X. Zhang, X. Zhu, G. Cao, A. Zunger, and D. S. Dessau, *Phys. Rev. B* **95**, 075118 (2017).
- [31] E. Paris, B. Joseph, A. Iadecola, T. Sugimoto, L. Olivi, S. Demura, Y. Mizuguchi, Y. Takano, T. Mizokawa, and N. L. Saini, *J. Phys.: Condens. Matter* **26**, 435701 (2014).
- [32] A. Athauda, J. Yang, S. Lee, Y. Mizuguchi, K. Deguchi, Y. Takano, O. Miura, and D. Louca, *Phys. Rev. B* **91**, 144112 (2015).
- [33] R. Sagayama, H. Sagayama, R. Kumai, Y. Murakami, T. Asano, J. Kajitani, R. Higashinaka, T. D. Matsuda, and Y. Aoki, *J. Phys. Soc. Jpn.* **84**, 123703 (2015).
- [34] G. M. Pugliese, F. Stramaglia, F. G. Capone, M. Y. Hacısalihoglu, R. Kiyama, R. Sogabe, Y. Goto, S. Pollastri, D. Oliveira, De Souza, L. Olivi, T. Mizokawa, Y. Mizuguchi, and N. L. Saini, *J. Phys. Chem. Solids* **147**, 109648 (2020).
- [35] N. L. Saini *et al.* (unpublished).
- [36] G. M. Pugliese, E. Paris, F. G. Capone, F. Stramaglia, T. Wakita, K. Terashima, T. Yokoya, T. Mizokawa, Y. Mizuguchi, and N. L. Saini, *Phys. Chem. Chem. Phys.* **22**, 22217 (2020).
- [37] E. Paris, Y. Mizuguchi, M. Y. Hacısalihoglu, T. Hiroi, B. Joseph, G. Aquilanti, O. Miura, T. Mizokawa, and N. L. Saini, *J. Phys.: Condens. Matter* **29**, 145603 (2017).
- [38] M. Nagao, A. Miura, S. Watauchi, Y. Takano, and I. Tanaka, *Jpn. J. Appl. Phys.* **54**, 083101 (2015).
- [39] M. Nagao, A. Miura, R. Matsumoto, S. Watauchi, Y. Takano, and I. Tanaka, *Solid State Commun.* **296**, 17 (2019).
- [40] S. Ishii, Y. Hongu, A. Miura, and M. Nagao, *Appl. Phys. Express* **9**, 063101 (2016).
- [41] S. Dash, T. Morita, K. Kurokawa, Y. Matsuzawa, N. L. Saini, N. Yamamoto, J. Kajitani, R. Higashinaka, T. D. Matsuda, Y. Aoki, and T. Mizokawa, *Phys. Rev. B* **98**, 144501 (2018).
- [42] R. Jha, A. Kumar, S. K. Singh, and V. P. S. Awana, *J. Supercond. Novel Magn.* **26**, 499 (2013).
- [43] K. Shimada, M. Arita, T. Matsui, K. Goto, K. Yoshida, M. Taniguchi, H. Namatame, T. Sekitani, K. Tanaka, H. Yoshida, K. Shirasawa, N. Smolyakov, and A. Hiraya, *Nucl. Instrum. Methods Phys. Res., Sect. A* **467–468**, 504 (2001).
- [44] H. Iwasawa, K. Shimada, E. F. Schwier, M. Zheng, Y. Kojima, H. Hayashi, J. Jiang, M. Higashiguchi, Y. Aiura, H. Namatame, and M. Taniguchi, *J. Synchrotron Radiat.* **24**, 836 (2017).

- [45] P. Giannozzi *et al.*, *J. Phys.: Condens. Matter* **21**, 395502 (2009).
- [46] P. Giannozzi *et al.*, *J. Phys.: Condens. Matter* **29**, 465901 (2017).
- [47] T. Sugimoto, E. Paris, T. Wakita, K. Terashima, T. Yokoya, A. Barinov, J. Kajitani, R. Higashinaka, T. D. Matsuda, Y. Aoki, T. Mizokawa, and N. L. Saini, *Sci. Rep.* **8**, 2011 (2018).
- [48] N. P. Armitage, P. Fournier, and R. L. Greene, *Rev. Mod. Phys.* **82**, 2421 (2010).
- [49] N. P. Armitage, D. H. Lu, D. L. Feng, C. Kim, A. Damascelli, K. M. Shen, F. Ronning, Z.-X. Shen, Y. Onose, Y. Taguchi, and Y. Tokura, *Phys. Rev. Lett.* **86**, 1126 (2001).
- [50] M. Horio, T. Adachi, Y. Mori, A. Takahashi, T. Yoshida, H. Suzuki, L. C. C. Ambolode, K. Okazaki, K. Ono, H. Kumigashira, H. Anzai, M. Arita, H. Namatame, M. Taniguchi, D. Ootsuki, K. Sawada, M. Takahashi, T. Mizokawa, Y. Koike, and A. Fujimori, *Nat. Commun.* **7**, 10567 (2016).
- [51] M. Horio, S. Sakai, K. Koshiishi, Y. Nonaka, H. Suzuki, J. Xu, M. Hashimoto, D. Lu, Z.-X. Shen, T. Ohgi, T. Konno, T. Adachi, Y. Koike, M. Imada, and A. Fujimori, [arXiv:1801.04247](https://arxiv.org/abs/1801.04247).
- [52] E. H. da Silva Neto, R. Comin, F. He, R. Sutarto, Y. Jiang, R. L. Greene, G. A. Sawatzky, and A. Damascelli, *Science* **347**, 282 (2015).